Received: 2 May 2018 | Revised: 18 June 2018 | Accepted: 19 June 2018

DOI: 10.1002/jsp2.1025

JOR Spine OPEN ACCESS

RESEARCH ARTICLE

# Tgfbr2 is required in Acan-expressing cells for maintenance of the intervertebral and sternocostal joints

**Bashar Alkhatib | Cunren Liu | Rosa Serra**

Department of Cell, Developmental and Integrative Biology, University of Alabama at Birmingham, Birmingham, Alabama

**Correspondence**
Rosa Serra, Department of Cell, Developmental and Integrative Biology, University of Alabama at Birmingham, Birmingham, AL.
Email: rserra@uab.edu

**Funding information**
National Institute of Arthritis and Musculoskeletal and Skin Diseases, Grant/Award Number: R01 AR053860; National Institute of Dental and Craniofacial Research, Grant/Award Number: T90DE022736

**Background:** Members of the transforming growth factor beta (TGF-β) family are secreted proteins that regulate skeletal development. TGF-β signaling is critical in embryonic development of the annulus fibrosus (AF) of the intervertebral disc (IVD). To address the question of the role of TGF-β signaling in postnatal development and maintenance of the skeleton, we generated mice in which *Tgfbr2* was deleted at 2-weeks of age in Aggrecan (Acan)-expressing cells using inducible Cre/LoxP recombination.

**Methods:** Localization of Cre recombination was visualized by crossing $Acan^{tm1(cre/ERT2)Crm}$ mice to fluorescent mTmG reporter mice. $Acan^{tm1(cre/ERT2)Crm}$ mice were mated to $Tgfbr2^{LoxP/LoxP}$ mice and Cre recombinase was activated by tamoxifen injection at 2-weeks postnatally. Following tamoxifen injection, mice were aged to 3, 6, and 12-months and control mice were compared to the experimental (cKO) group. Mice were initially analyzed using X-ray and skeletal preparations. Sternocostal joints and IVD tissues were further analyzed histologically by hematoxylin and eosin (H&E), Safranin O, and Picrosirius Red staining as well as Col10 immunostaining.

**Results:** Cre recombination was observed in the IVD and sternocostal joints. X-ray analysis revealed osteophyte formation within the disc space of 12-month-old cKO mice. Skeletal preparations confirmed calcification within the IVD and the sternocostal joints in cKO mice. H&E staining of cKO IVD revealed disorganized growth plates, delay in the formation of the bony endplate, and Col10 staining in the AF indicative of ectopic endochondral bone formation. Furthermore, proteoglycan loss was observed and collagen bundles within the inner AF were thinner and less organized. Alterations in the IVD were apparent beginning at 3 months and were progressively more visible at 6 and 12 months. Similarly, histological analysis of cKO sternocostal joints revealed joint calcification, proteoglycan loss, and disorganization of the collagen architecture at 12 months of age.

**Conclusions:** TGF-β signaling is important for postnatal development and maintenance of fibrocartilaginous IVD and sternocostal joints.

KEYWORDS

annulus fibrosus, end plate, growth plate, intervertebral disc, sternum

## 1 | INTRODUCTION

Transforming growth factor beta (TGF-β) is a multifunctional growth factor that regulates various aspects of development, cell differentiation, extracellular matrix (ECM) deposition, and tissue homeostasis.[1,2] The TGF-β family consists of several members including three TGF-β ligands (TGF-β1, 2, and 3), activins and inhibins, growth and differentiation factors (GDFs), and bone morphogenetic proteins (BMPs).[3] TGF-β signaling occurs through TGF-β receptors that bind the ligand at the cell surface. Previous literature has demonstrated through biochemical and genetic evidence that both the TGF-β type I and type II receptors (Tgfbr1 and Tgfbr2) are necessary to generate a response to TGF-

β.[4–6] The current accepted model is that, initially, the ligand binds to Tgfbr2 at the cell surface.[7] The Tgfbr2 recruits Tgfbr1 to form a heterotetrameric complex with one additional Tgfbr1 and Tgfbr2.[7] The Tgfbr2 is a constitutively active kinase and it phosphorylates the GS domain of Tgfbr1.[7] This activates the Type I serine/threonine kinase and allows downstream targets to transduce the signal to the nucleus.[7]

The intervertebral disc (IVD) is a fibrocartilaginous joint in the spine. Positioned between two bony vertebral bodies, the IVDs serve mainly to resist axial compression on the spine and to provide a range of motion.[8–10] The IVD consists of two primary regions, the nucleus pulposus (NP) and the annulus fibrosus (AF).[8–10] The NP is derived from the notochord and the AF is derived from sclerotome.[11] The NP and AF are composed of collagens and proteoglycans, such as collagens I and II and aggrecan with the NP having very high proteoglycan and water content relative to the AF.[8–10] The mouse sternum also has a fibrocartilage joint in between each sternebrae, where the sternum and ribs connect called the sternocostal joint (SJ). In humans the sternebrae fuse in young adults to form the body of the sternum; however, this joint is maintained in mice.

Alterations in the expression or function of TGF-β ligands and their receptors have been described in the pathological states of several skeletal tissues, including the axial skeleton. For example, association between a SNP in the *TGFB1* gene and spinal osteophytosis and scoliosis have been reported.[12,13] Alterations in the *TGFB3* or *TGFBR2* genes are associated with cervical instability and scoliosis observed in Loeys-Dietz Syndrome.[14–16] Polymorphisms in the *TGFB3* or *TGFBR2* genes are also associated with ossification of the posterior longitudinal ligament in the spine.[17,18] In addition, polymorphisms in CILP, an extracellular regulator of TGF-β function, are associated with Lumbar Disc Disease.[13]

Previous studies using mouse models have also highlighted the importance of TGF-β signaling in skeletal development and homeostasis.[19] Expression of a truncated, kinase defective *Tgfbr2* in mouse skeletal tissue resulted in articular chondrocyte hypertrophy and osteoarthritis of the knee joint.[20] Furthermore, progressive skeletal degeneration was observed in these mice and vertebra of the spine were often misshapen and appeared fused.[20] Targeted conditional deletion of *Tgfbr2* embryonically in Col2a1-expressing cells in mice caused more specific skeletal deformities in mice including incomplete development and disorganization of the AF.[21] Few studies have investigated the role of TGF-β signaling in the postnatal growth and maintenance of the IVD. One study conditionally deleted *Tgfbr2* using Col2a1$^{tm1(cre/ERT2)}$ in mice at 2-weeks postnatally by tamoxifen injection.[22] This study reported disrupted columnar structure and loss of chondrocytes within the vertebral growth plates (GPs) as well as defects in the growth and maintenance of the cartilage endplates at 3 months of age.[22] Aged mice were not characterized. These observations warrant further investigation of not only the role of TGF-β ligands and receptors during postnatal development, but also their role in maintaining the IVD.

In this study, we use Acan$^{tm1(cre/ERT2)Crm}$ to delete *Tgfbr2* in the axial skeleton. Cre was activated by tamoxifen injection when the mice were 2-weeks of age. Cre activity was detected using an mTmG reporter. Activity was detected in GP and iAF, similar to what was previously observed using Col2a1$^{tm1(cre/ERT2)}$ -mediated deletion.[22] In contrast, activation of Acan$^{tm1(cre/ERT2)Crm}$ was also observed in the endplates and in the NP. Deletion of *Tgfbr2* in Acan$^{tm1(cre/ERT2)Crm}$ expressing cells resulted in discontinuous and disorganized GP, similar to that observed in the Col2a1$^{tm1(cre/ERT2)}$ *Tgfbr2*-deleted mice. However, aged Acan$^{tm1(cre/ERT2)Crm}$; *Tgfbr2*$^{LoxP/LoxP}$ mice demonstrated inappropriate hypertrophic differentiation at the junction of the iAF, endplate and GP, that likely resulted in bony bridges that were detected in skeletal preparations and X-ray images. A delay in the formation of the bony endplate was also seen. In addition, matrix changes were observed in the IVD of Acan$^{tm1(cre/ERT2)Crm}$; *Tgfbr2*$^{LoxP/LoxP}$ mice; proteoglycans were reduced in all regions of the IVD and collagen disorganization was observed in the iAF. Furthermore, joint collapse, proteoglycan loss, and collagen disorganization were observed in fibrocartilaginous joints in the sternum. This study indicates that TGF-β signaling is important for the postnatal development and maintenance of fibrocartilage joints.

## 2 | MATERIALS AND METHODS

### 2.1 | Transgenic mouse model

All animal work was approved and carried out in accordance with the guidelines and policies of the University of Alabama at Birmingham Institutional Animal Care and Use Committee.

Acan$^{tm1(cre/ERT2)Crm}$ (JAX stock #019148)[23] and *Tgfbr2*$^{LoxP/LoxP}$ mice were generated as previously described.[24] Acan$^{tm1(cre/ERT2)Crm}$ mice were mated to *Tgfbr2*$^{LoxP/LoxP}$ mice to generate Acan$^{tm1(cre/ERT2)Crm}$;*Tgfbr2*$^{WT/LoxP}$ mice. Acan$^{tm1(cre/ERT2)Crm}$;*Tgfbr2*$^{WT/LoxP}$ mice were then crossed with *Tgfbr2*$^{LoxP/LoxP}$ mice to generate Acan$^{tm1(cre/ERT2)Crm}$; *Tgfbr2*$^{LoxP/LoxP}$ mice (denoted as cKO in this article) which were the mice utilized as the experimental group. *Tgfbr2*$^{LoxP/LoxP}$ or *Tgfbr2*$^{WT/LoxP}$ mice were utilized as the control group (denoted as CTL in this article). Both Acan$^{tm1(cre/ERT2)Crm}$ and *Tgfbr2* $^{LoxP/LoxP}$ strains are in the C57BL/6 background.

The genotype of transgenic mice was determined by polymerase chain reaction (PCR) analysis of DNA isolated from mouse tail tissue. DNA was released from tail tissue using Proteinase K digestion and then isolated using phenol/chloroform extraction. PCR was performed on the Cre transgene using the following primers: Cre5′ (TGC TCT GTC CGT TTG CCG) and Cre3′ (ACT GTG TCC AGA CCA GGC). Three primers were used to detect the presence and deletion of Tgfbr2 exon 2. The loxP allele was identified using the following primers: 8w-a (TAA ACA AGG TCC GGA GCC CA) and LA-loxP (ACT TCT GCA AGA GGT CCC CT). Two bands were detected using these primers. One band represents the wild-type allele (420 bp) and the other represents the loxP (flox) allele (540 bp). The presence of both bands indicated that a mouse is heterozygous for the loxP allele. In order to confirm whether recombination and deletion of *Tgfbr2* exon 2 (loss of the floxed allele) had occurred, the following primers were used: CIdelR (AGA GTG AAG CCG TGG TAG GT). Successful recombination and loss of *Tgfbr2* exon 2 was confirmed by the presence of a 610 bp band. mTmG mice were genotyped using three separate primers: Wild-type Forward (CTC TGC TGC CTC CTG GCT TCT),

Wild-type Reverse (CGA GGC GGA TCA CAA GCA ATA), and Mutant reverse (TCA ATG GGC GGG GGT CGT T). These primers detect two bands, a 330 bp band and a 250 bp band. The presence of the 330 bp band indicated a wild-type mouse with no tomato reporter gene expression. Mice that expressed the tomato reporter gene insert had either the 250 bp band alone (homozygous) or both the 330 and 250 bp bands together (heterozygous). Only one allele is required to observe ubiquitous tomato reporter gene expression. Genomic DNA was amplified for 30 cycles of denaturation at 94°C for 30 seconds, annealing at 55°C for 40 seconds, and elongation at 72°C for 40 seconds. Reactions were performed in a reaction buffer containing 1.5 mM $MgCl_2$, 1× PCR buffer (Denville Scientific, Inc., Holliston, MA), 0.4 mM dNTPs (Invitrogen, Waltham, MA), Choice Taq Blue DNA polymerase (Denville Scientific, Inc.), and 0.4 mM of each primer.

## 2.2 | Tamoxifen injection

Tamoxifen (T5648, Sigma-Aldrich, St. Louis, MO) was dissolved in sterile sunflower oil at a concentration of 10 mg/mL and agitated to ensure full dissolution. Mice were injected with 1.7 mg of tamoxifen per 10 g of body weight at 2 weeks of age. Three separate intraperitoneal injections (one injection every other day) were performed. Tamoxifen and sunflower oil mixtures were protected from light and stored at −20°C until use.

## 2.3 | Localization of Cre expression

Gt(ROSA)$^{26Sortm4(ACTB-tdTomato,-EGFP)Luo}$ (mTmG) (JAX stock #007676)[25] mice heterozygous for the loxP flanked tdTomato cassette were crossed to Cre-positive Acan$^{tm1(cre/ERT2)Crm}$ mice. The membrane-targeted tdTomato red fluorescent reporter is expressed in all tissues and cell types. This tdTomato cassette is deleted in cells where Cre recombination occurs, allowing for the downstream membrane-targeted green fluorescent reporter (EGFP) to be expressed. All littermates were injected with tamoxifen at 2 weeks of age and sacrificed at 4 weeks of age to examine skeletal joint tissue for cre expression. Cre-negative mice ($n$ = 3) were compared to Cre-positive mice ($n$ = 3) and all mice examined expressed tdTomato reporter. Skeletal tissues from 4-week old mice were fixed in 4% paraformaldehyde (Cat#15714-S, Electron Microscopy Sciences, Hatfield, PA) for 1 hour. Tissues were placed in successive overnight incubations in 10%, 20%, and 30% sucrose at 4°C. This was followed by an overnight incubation in a 1:1 solution of 30% sucrose and optimal cutting temperature (OCT) compound (Cat#25608-930, VWR, Radnor, PA). Samples were embedded in disposable base molds in 100% OCT compound and flash frozen in preparation for sectioning. Frozen tissue blocks were cryosectioned on a Leica Jung Frigocut 2800E Buffalo Grove, IL and 10-μm thick tissue sections were placed on glass slides. Tissue sections were rehydrated with distilled water and then incubated in a 1-μg/mL working solution of DAPI (Cat# 62248, Thermo Scientific, Waltham, MA) for 10 minutes and then washed with PBS. Slides were all mounted with Aqua Poly/Mount (Cat# 18606-20, Polyscience, Inc., Warrington, PA), an aqueous mounting medium, and covered with glass cover slips. Fluorescent imaging was performed on a. Olympus BX51 fluorescent microscope. Images were processed using cellSens imaging software (Center Valley, PA).

Cre recombination efficiency was calculated by counting the number of Cre-positive (GFP) and Tomato-positive (RFP) cells in the NP, iAF, oAF, GP, and CEP regions. Within each individual region, GFP and RFP cell numbers were added together (total cell number) and the GFP number was divided by the total number of cells and multiplied by 100 to obtain a percentage. Cell counts were averaged for each region from each of three different mice (Cre-positive progeny from Acan$^{tm(IRES-creERT2)/+}$;mTmG$^{+/-}$ crosses) and counted from a single section from each mouse.

## 2.4 | Radiographic imaging

One-year old mice (control $n$ = 7, cKO $n$ = 5) were anesthetized using a table-top isoflurane anesthesia vaporizer machine. Mice were subjected to a mixture of oxygen (flow rate of 500 mL per minute) and 3% isoflurane for 10 to 15 minutes until they were sedated. Dorsolateral X-rays of the spine were performed on a Faxitron MX-20-DC4 (Tuscon, AZ) small animal X-ray machine managed by the Small Animal Phenotyping Core at UAB. Images were processed using the Specimen System software (Tuscon, AZ).

## 2.5 | Skeletal preparations

Skeletal preparations were performed as described previously.[26] Briefly, 1-year old mice (control $n$ = 3, cKO $n$ = 3) were skinned, eviscerated, and covered with a 1% solution of potassium hydroxide (P1767, Sigma-Aldrich, St. Louis, MO) for 7 days. Subsequently, skeletons were then covered with a 2% potassium hydroxide solution for 1 day and then covered with a 1.9% solution of potassium hydroxide containing alizarin red S (A5533, Sigma-Aldrich, St. Louis, MO) for 2 days. Skeletons were cleared for 4 days using a solution containing 40% glycerol (G6279, Sigma-Aldrich, St. Louis, MO), 20% benzyl alcohol (A395, Fisher Scientific, Hampton, NH), and 40% anhydrous ethanol (Cat#2701, Decon Laboratories (King of Prussia, PA)). Skeletons were stored in glycerol until imaging. Imaging was performed using an Olympus SZX12 dissection microscope (Center Valley, PA). Leica software (Buffalo Grove, IL) was used to process images.

## 2.6 | Tissue preparation

Rib cages and spines were dissected from 3-month, 6-month, and 1-year old mice (control $n$ = 3 and cKO $n$ = 3 within each tissue and each age group, $n$ = biological replicates meaning sections from individual mice). All incubations in the tissue preparation procedure were performed with end-over-end agitation at 4°C. Skeletal organs were fixed in 4% paraformaldehyde overnight. Subsequently, organs were dehydrated in separate overnight washes of 70%, 80%, 95%, and 100% ethanol. This was followed by overnight incubations in xylene at room temperature, paraffin wax:xylene (50:50) at 60°C, and paraffin wax alone at 60°C. Skeletal organs were embedded in paraffin wax using a plastic mold and allowed to harden at room temperature. Paraffin blocks were sectioned using a Reichert-Jung 2030 biocut microtome (Depew, NY) and 6-μm thick sections were captured on glass slides. Slides were warmed on heaters at 50°C for 1 hour to flatten tissue sections. Slides were stored at 4°C until staining and analysis.

### 2.7 | H&E staining

Tissue slides were deparaffinized in two washes of xylene for 5 minutes each and rehydrated in two washes of both 100% ethanol and 90% ethanol for 3 minutes each. Following a 3 minute rinse in distilled water, slides were placed in Harris modified hematoxylin solution (SH26, Fisher Chemical, Hampton, NH) for 2 minutes. Slides were then rinsed in tap water, dipped in 70% ethanol containing 0.25% HCl, rinsed in tap water once again, and immersed in Eosin Y solution (HT110132, Sigma-Aldrich, St. Louis, MO) for 3 minutes. Slides were rehydrated with two 3 minute washes each of 90% and 100% ethanol and two final 5 minute washes of xylene. Slides were mounted with three to five drops of Cytoseal-60 (ref#8310-4, Thermo Scientific, Waltham, MA), a resin-based mounting medium, and sealed with coverslips. Slides were imaged on an Olympus BX51 microscope and images were processed using cellSens Standard imaging software.

### 2.8 | Safranin-O staining

Slides were deparaffinized and rehydrated in two washes of xylene for 5 minutes each, two washes of 100% ethanol for 2 minutes each, and one wash of 90% ethanol for 2 minutes. After a rinse with distilled water, slides were immersed in 0.05% Fast Green FCF solution (F7259, Sigma-Aldrich, St. Louis, MO) for 5 minutes. This was followed by a rinse in 1% acetic acid solution. Slides were immersed in 0.1% Safranin-O solution (S8884, Sigma-Aldrich, St. Louis, MO) and then dehydrated in two washes each of 90% ethanol, 100% ethanol, and xylene for 2 minutes each. Slides were mounted and imaged as described in the previous section.

### 2.9 | Picrosirius red staining

Slides were deparaffinized and rehydrated with two washes of xylene for 5 minutes each and two washes of 100%, 90%, 80%, and 70% ethanol for 3 minutes each. Slides were directly immersed in a 500 mL saturated aqueous solution of picric acid (SP9200, Fisher Scientific Hampton, NH) containing 0.5 g of Sirius Red F3B (Direct Red 80) (26-10-8, Sigma-Aldrich, St. Louis, MO) for 1 hour. This was followed by two washes in acidified water (5 mL of acetic acid in 1 L of water) for 5 minutes each. Water was then removed from all slides by vigorous shaking and blotting with tissue paper. Slides were dehydrated in three changes of 100% ethanol. Tissue specimens were mounted on slides using resinous mounting media and glass coverslips. Specimens were viewed under polarized light using an Olympus BX51 microscope with two separate attachments: a transmitted light analyzer (U-ANT, 3812700, Olympus, Japan) and a drop-in polarizer (U-POT, 3812600, Olympus, Japan). Images were processed using cellSens Standard imaging software.

### 2.10 | Immunohistochemistry

Tissue slides were deparaffinized in two changes of xylene for 5 minutes each. Slides were rehydrated in two washes of 100% ethanol for 3 minutes each and one wash of 95% ethanol for 3 minutes. Endogenous peroxidase activity was blocked by washing slides in 3% hydrogen peroxide in methanol for 10 minutes. For Col10 staining, after two 5 minute washes in phosphate buffered saline (PBS), enzymatic antigen retrieval was performed on all tissue slides with Proteinase K solution. Tissue slides were incubated in 0.2 mg/mL proteinase K solution (buffer contents: 2 M Tris pH 8.0, 0.5 M Ethylenediaminetetraacetic acid (EDTA) pH 8.0, 10% Sodium dodecyl sulfate (SDS), and 5 M NaCl) at room temperature for 10 minutes. For, Acan staining antigen retrieval was performed with citrate buffer. Sections were covered in citrate buffer (10 mM citric acid, 2 mM EDTA 0.05% Tween-20; pH 6.2) and microwaved for 1 minute 30 seconds at 50% power. This heating procedure was repeated four times with 30 second intermissions. This was followed by two 5 minutes washes in PBS. Tissue sections were incubated for 1 hour at room temperature in a blocking solution containing 5% bovine serum albumin (BSA) and 5% goat serum in Tris buffered saline with Tween-20 (TBS-T) (buffer contents: 200 mM Tris base, 1.5 M NaCl, 20 mM KCl, 1% Tween-20). After three washes for 5 minutes each in TBS-T, tissue sections were placed in primary antibody solution. A Col10 antibody (ab58632, AbCam, Cambridge, MA) was diluted to a 1:1000 concentration in 1% BSA, Acan antibody (Millipore, CAT# AB1031, Burlington, MA) was diluted to a 1:100 concentration and placed on tissue sections in a humidified chamber. Tissue sections were incubated in primary antibody overnight at 4°C. After three washes for 5 minutes each of TBS-T, tissue sections were incubated in a goat anti-rabbit HRP-linked secondary antibody (sc-2030, Santa Cruz Biotechnology, Dallas, TX) diluted to a 1:1000 concentration in 1% BSA solution. After 1 hour at room temperature, three times for 5 minutes each were performed with TBS-T. Tissue sections were exposed using an ImmPACT DAB kit (sk-4105, Vector Laboratories, Burlingame, CA) and then washed three times for 5 minutes each with distilled water. Slides were dehydrated in 95% and 100% ethanol and then cleared in two washes of xylene for 5 minutes each. Slides were mounted with a resinous mounting medium and sealed with coverslips as described in the 'H&E staining' section. Imaging was performed as described in the 'H&E staining' section.

## 3 | RESULTS

### 3.1 | Postnatal deletion of *Tgfbr2* in Acan$^{tm(IRES\text{-}creERT2)}$-expressing cells results in ectopic calcification and osteophyte formation in sternum and IVD

TGF-β signaling is critical for embryonic development of the IVD, specifically the AF.[21] In contrast, little is known about the role of TGF-β signaling in postnatal development and maintenance of the adult axial skeleton. To evaluate the role of TGF-β signaling in skeletal tissues, both *Tgfbr2*$^{WT/Lox\ or\ LoxP/LoxP}$ (CTL) and Acan$^{tm(IRES\text{-}creERT2)/-}$; *Tgfbr2*$^{LoxP/LoxP}$ (cKO) mice were injected with tamoxifen at 2-weeks of age to delete *Tgfbr2* after the tissues of the axial skeleton have initially formed. Mice were aged to 1-year and skeletal tissue was analyzed. Overall, both male and female cKO mice were smaller in size compared to CTL mice of a similar age. Initially, radiographic imaging analysis detected calcified tissue in the disc space of cKO mice (Figure 1A; bottom image, white arrows). Furthermore, mild thoracic and sacral kyphosis were observed in cKO mice (Figure 1A; bottom image, yellow arrow and red arrow, respectively). To extend the results of the radiographic analysis, Alizarin

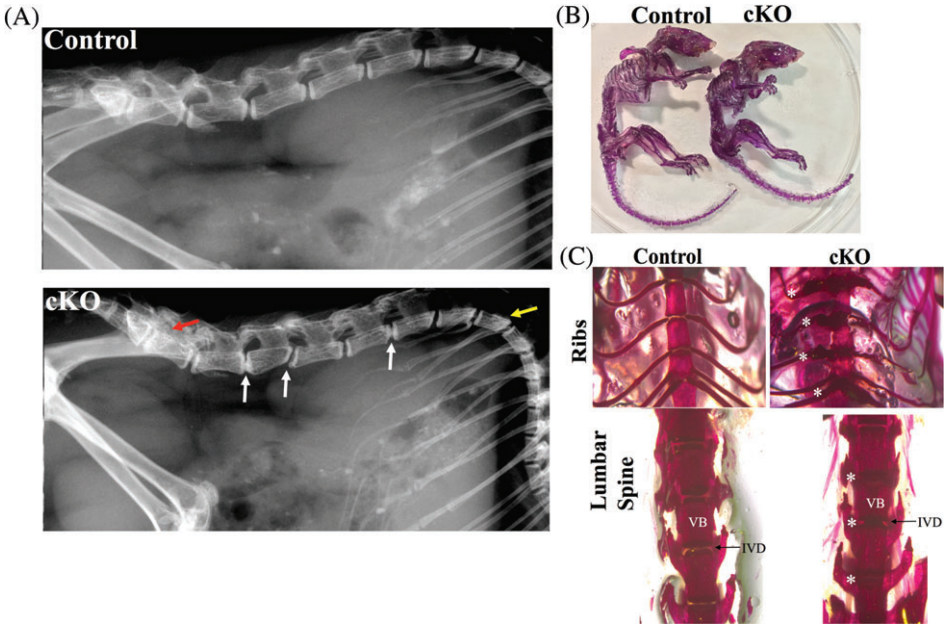


**FIGURE 1** Osteophyte formation in axial joints of Acan$^{tm(IRES\text{-}creERT2)}$ *Tgfbr2*$^{LoxP/LoxP}$ mice. Tgfbr2 was deleted in aggrecan-expressing cells postnatally by injecting *Tgfbr2*$^{LoxP/LoxP}$ or *Tgfbr2*$^{WT/LoxP}$ (CTL) and Acan$^{tm(IRES\text{-}creERT2)/+}$; *Tgfbr2*$^{LoxP/LoxP}$ (cKO) littermates with tamoxifen at 2-weeks of age. Mice were aged to 1-year and then skeletal tissue was analyzed. (A) Dorsolateral radiographic images of CTL and cKO mice at 1-year of age. Osteophyte formation was observed in cKO mice in the lumbar intervertebral disc (IVD) joint spaces (white arrows) and not in CTL IVDs. Mild kyphosis is also observed in the thoracic (yellow arrow) and sacral (red arrow) regions in cKO mice. (B) Alizarin red skeletal staining of 1-year old WT and cKO mice. (C) High magnification images of sternum and ribs (top) and lumbar IVDs (bottom) of 1-year old CTL and cKO mice. Alizarin red-stained, calcified tissue was observed in the joints of the sternum (white asterisks) and lumbar IVD (white asterisks) of cKO mice and not in CTL skeletal tissue

red skeletal preparations were generated from CTL and cKO mice (Figure 1B). Skeletal malformations were observed in cKO skeletons when compared to CTL (Figure 1B). Most notably, Alizarin red staining was observed in SJ (Figure 1C, white asterisks) and in the lumbar IVD spaces (Figure 1C, white asterisks) of cKO mice. The radiographic and whole mount observations are indicative of osteophyte formation in the joint spaces in the axial skeleton which was consistently observed in aged cKO mice but not in CTL.

## 3.2 | Cre recombination occurs in Acan$^{tm(IRES\text{-}creERT2)}$-expressing cells of the IVD and sternal joints

Cre activity has not previously been characterized in axial skeleton of Acan$^{tm(IRES\text{-}creERT2)/-}$ mice. To determine which cell types were potentially affected by deletion of *Tgfbr2* in these mice, we characterized Cre activity in the axial skeleton using an mTmG reporter. Acan$^{tm(IRES\text{-}creERT2)/-}$ mice were crossed to mTmG$^{+/-}$ reporter mice and Cre activity was induced with tamoxifen at 2-weeks of age then the mice were aged to 1 month. Skeletal tissues of Acan$^{tm(IRES\text{-}creERT2)/-}$;mTmG$^{+/-}$ mice were characterized by fluorescent microscopy to identify where Cre recombinase was active. In this reporter strain, cells in which Cre recombination occurs fluoresce green (GFP), otherwise cells fluoresce red (RFP). Cre recombination occurred within the IVD in several regions. Recombination efficiency was calculated as the percentage of cells expressing the GFP marker for each tissue (Table 1). Cre activity was detected within the NP, inner AF (iAF), the cartilaginous endplate (CEP), and the GP (Figure 2A,B). Less recombination occurred in the outer AF (oAF) or adjacent spinal ligaments (Figure 2A,B). This is in agreement with previous observations that Aggrecan is not expressed or expressed at very low levels in the ligaments and oAF.[27,28] Immunohistochemistry of Acan core protein indicated extensive overlap in tissues with Cre activity (Figure 2C). Furthermore, Cre activity was detected within the sternum and ribs of Acan$^{tm(IRES\text{-}creERT2)/-}$; mTmG$^{+/-}$ mice. More specifically, recombination occurred in the SJ, sternal GPs, and costal cartilage (CC) (Figure 2D). To confirm the efficacy of Cre activation by tamoxifen injection, the knee joint, another cartiaginous tissue abundant in aggrecan, was analyzed (Figure 2E). Cre expression was detected within the articular cartilage (AC) and the meniscus (MS) of the knee joint (Figure 2E).

Not only was Cre activity detected in these tissues using the fluorescent reporter, but *Tgfbr2* exon2 was deleted. DNA was isolated from 1-year old IVD and sternum from wild type and Acan$^{tm(IRES\text{-}creERT2)/-}$; *Tgfbr2*$^{LoxP/LoxP}$ mice. Cre primers that recognize the Cre transgene were used to detect the presence or absence of Cre DNA. For *Tgfbr2*, three primers were used to detect the presence or absence of wild type, *Tgfbr2*

**TABLE 1** Cre recombination efficiency in IVD tissues

| Region | Percent GFP+ cells (%) |
|---|---|
| Nucleus pulposus | 98 |
| Inner annulus fibrosus | 93 |
| Outer annulus fibrosus | 21 |
| Cartilaginous endplate | 95 |
| Growth plate | 70 |

Abbreviation: GFP, green fluorescent reporter.

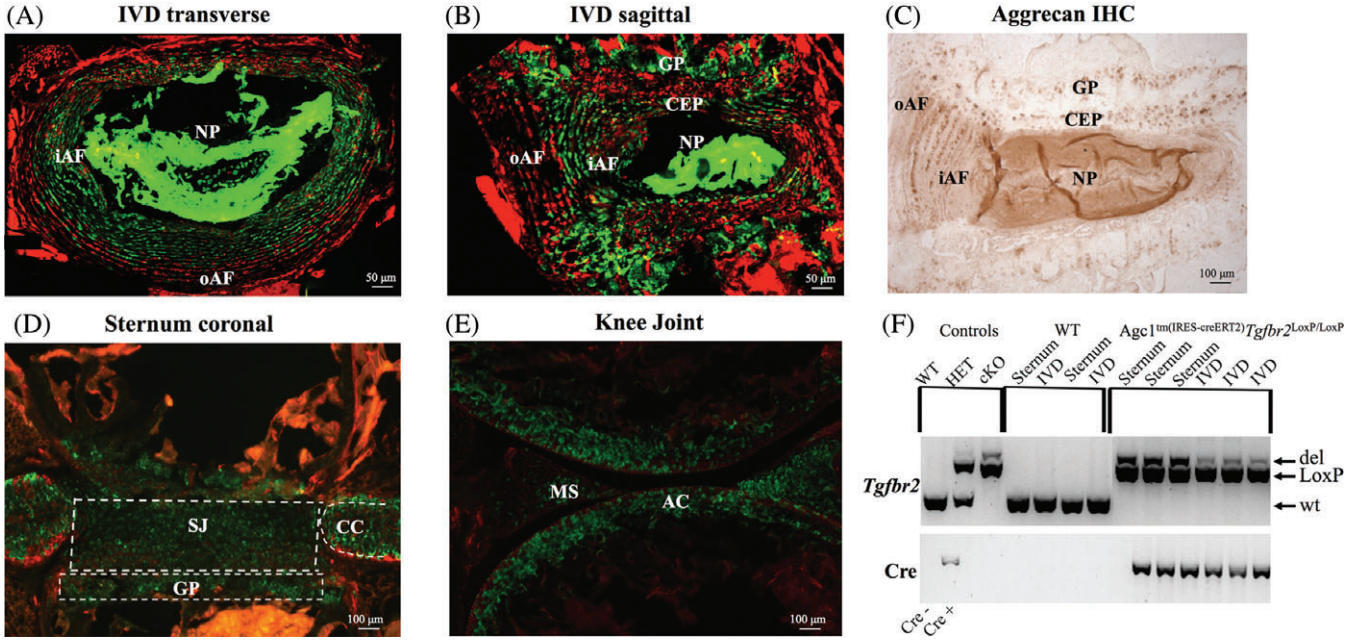


**FIGURE 2** Acan$^{tm(IRES\text{-}creERT2)}$ is active and *Tgfbr2* exon 2 is deleted in the sternum and intervertebral disc (IVD). Acan$^{tm(IRES\text{-}creERT2)/+}$;mTmG$^{+/-}$ mice were injected with tamoxifen at 2-weeks of age. Cre recombination occurred in cells that are labeled with green fluorescent protein (GFP) and did not occur in cells labeled with red fluorescent protein (tdTomato). (A,B) Fluorescent image composites of transverse (A) and sagittal (B) sections from lumbar IVD are shown. Cre activity is seen in the nucleus pulposus (NP), inner annulus fibrosus (iAF), cartilaginous endplate (CEP), and growth plate (GP). Few cells with Cre activity were detected in the outer annulus fibrosus (oAF). VB, vertebral body. (C) Immunohistochemical staining for aggrecan performed on a sagittal section of a 1-year old control IVD. (D) Coronal sections of the sternum showed Cre activity in the costal cartilage (CC), the sternocostal joint (SJ), and growth plate of sternebrae (GP). (E) Sagittal section of a knee joint from an mTmG reporter mouse. Cre activity is detected in the articular cartilage (AC) and the meniscus (MS). (F) PCR detection of tissue specific deletion of *Tgfbr2* exon 2. DNA was isolated from IVDs and sternum of 1-year old WT and cKO mice. The Cre transgene was detected by PCR. Detection of various alleles of *Tgfbr2* exon 2 was performed by PCR. Wild-type (wt) allele is represented as a 420 bp band, LoxP allele is 540 bp, and the *Tgfbr2* deleted allele (del) is 610 bp

exon 2 deletion, or the floxed allele. The localization of these primers was previously described.[29] Deletion of *Tgfbr2* exon 2 was demonstrated by the presence of a 610 bp band (Figure 2F, del). The wild-type allele appeared as a 420 bp band (Figure 2F, wt) and the floxed *Tgfbr2* allele with LoxP sites flanking exon 2 appeared as a 540 bp band (Figure 2F, LoxP). All Acan$^{tm(IRES\text{-}creERT2)/-}$; *Tgfbr2*$^{LoxP/LoxP}$ samples demonstrate the presence of the deleted allele and LoxP allele (Figure 2F). A possible reason for the persistent presence of the LoxP allele is the heterogeneity of Cre recombination within various tissues as indicated in Table 1. Specifically, Cre recombination does not occur in some cells, therefore deletion of *Tgfbr2* exon 2 will not occur leaving the LoxP allele in those cells. This can also explain the difference in the level of deletion between the IVD samples and the sternum samples. Nonetheless, wild-type tissues only showed the presence of the WT band and did not contain Cre DNA (Figure 2F). Cre transgene was evident in all cKO samples (Figure 2F).

## 3.3 | IVD structure is disrupted in cKO mice

Previous studies have demonstrated that TGF-β signaling is critical for the proper embryonic development of the IVD.[20,21,30,31] Embryonic deletion of *Tgfbr2* in collagen II-expressing cells caused incomplete development of the IVD.[21] To characterize the effects of loss of *Tgfbr2* on postnatal IVD, paraffin-embedded sections of 3-, 6-, and 12-month-old lumbar spines from mice that were treated with tamoxifen at 2-weeks were stained with hematoxylin and eosin (H&E) (Figures 3 and 4). In 3-month cKO IVDs, some phenotypic changes were evident. The most notable was that the GP was disorganized and discontinuous in the mutants, whereas the GP in the controls was straight and ran across the entire width of the vertebrae (Figure 3D,E). In addition, the cells within the mutant GP were not aligned into columns and formed clusters in some places (Figure 3E, black arrows). Control mice demonstrated both cartilaginous and bony endplates in between the GP and the annulus of the IVD; however, bony endplates were not detected in mutant mice (Figure 3B,C). By 6 months of age, the GP in the *Tgfbr2* cKO mice was highly disorganized and discontinuous (Figure 3J, black arrows). Most of the endplates in the control mice were bony while the end plates in mutant mice were still cartilaginous (Figure 3F). The iAF in control mice had a lamellar structure that appeared fibrous with small elongated cells (Figure 3G). In contrast, the cells within the iAF in the mutant mice were round the tissue and the fibrous or lamellar organization of the tissue was not clear (Figure 3H). In addition, the lateral junction of the iAF, end plate and GP contained clusters of disorganized round cells embedded in matrix resembling hyaline cartilage (Figure 3H, black arrow) and suggestive of endochondral bone formation. At 12-months of age, similar phenotypic changes were observed as at 6 months (Figure 4A); disorganized and discontinuous GPs (Figures 4E yellow arrows), delay in the formation of the bony endplate (Figure 4D, black arrow), round cells in the iAF and tissue without sharp lamellar structure (Figure 4D, red arrow).

To further characterize the phenotype of these cells and test the hypothesis that inappropriate hypertrophic differentiation at the junction

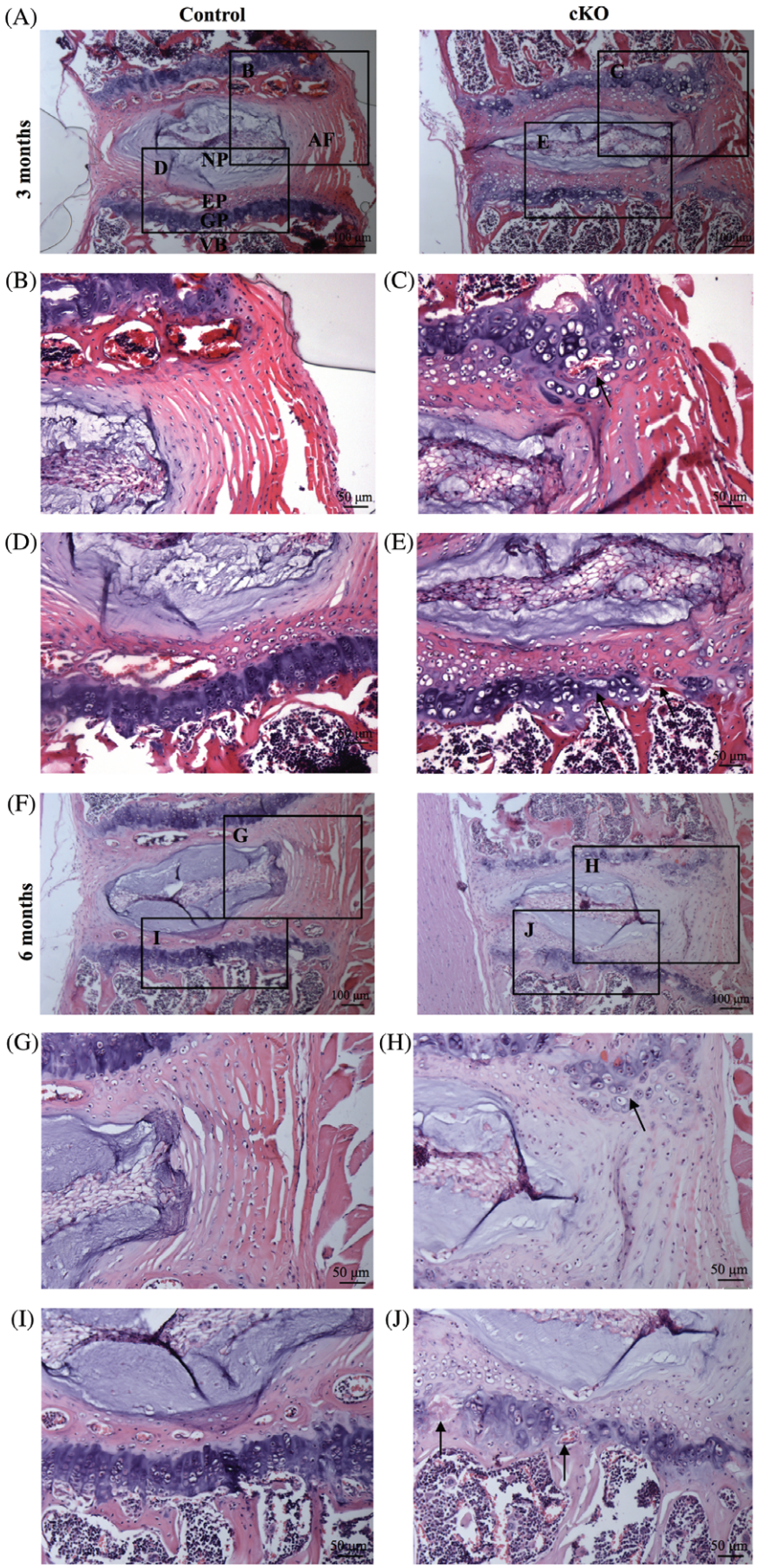


**FIGURE 3** Phenotypic alterations in Acan$^{tm(IRES\text{-}creERT2)}$ *Tgfbr2*$^{LoxP/LoxP}$ intervertebral disc (IVD) at 3 and 6-months. IVD tissue was isolated from 3- (A-E) and 6-month-old (F-J) control (A, B, D, F,G, I) and cKO (A, C, E, F, H, J) mice. Paraffin-embedded sagittal sections were stained with hematoxylin and eosin (H&E). Low magnification images are shown in A and F. Higher magnification images of boxes from A and F are indicated. Abnormal presence of hypertrophic cells is shown in C and H (black arrows). Disorganization and non-continuous growth plate shown in E and J (black arrows). Normal elongated cell morphology was observed in the AF region in B and G compared to round cells in cKO in C and H. NP, nucleus pulposus; AF, annulus fibrosus; EP, endplate; GP, growth plate; VB, vertebral body

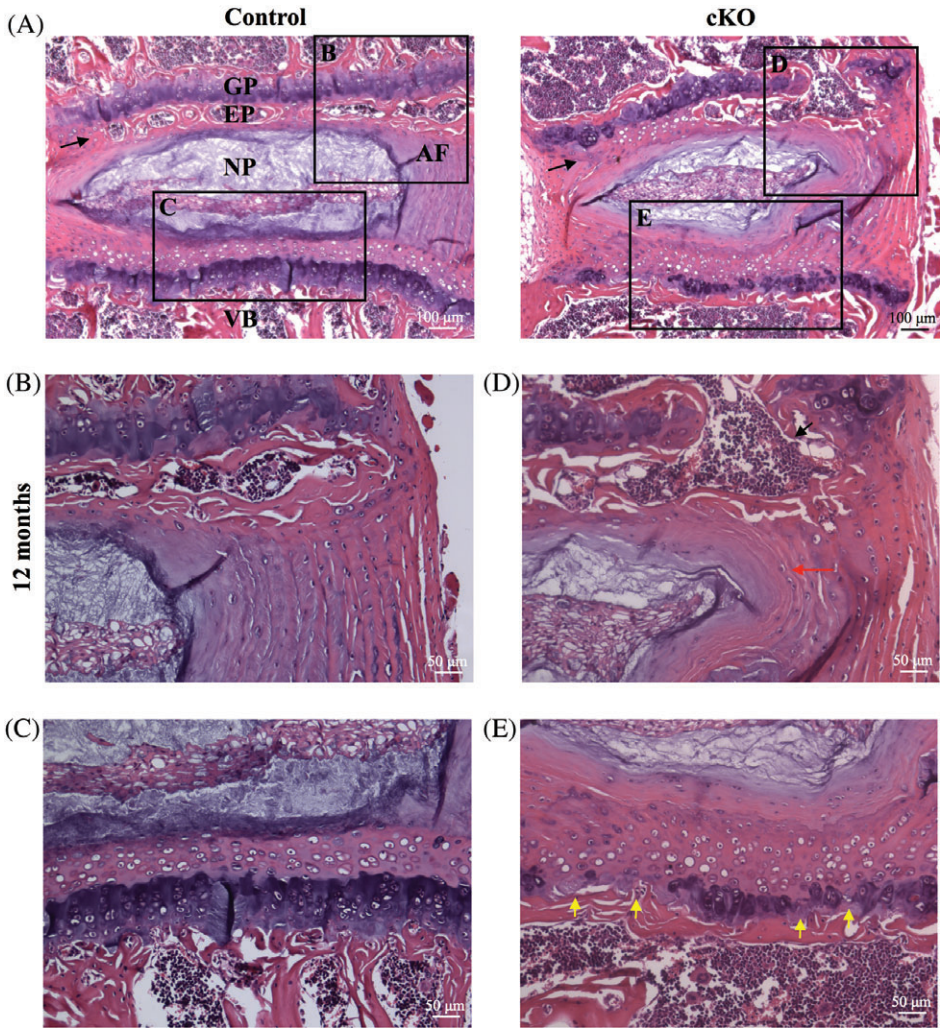


**FIGURE 4** Phenotypic alterations in Acan$^{tm(IRES\text{-}creERT2)}$ *Tgfbr2*$^{LoxP/LoxP}$ intervertebral disc (IVD) at 12-months. IVD tissue was isolated from 12-month-old control (A-C) and cKO (A, D, E) mice. Paraffin-embedded sagittal sections were stained with hematoxylin and eosin (H&E). (A) Low magnification images of H&E stained control and cKO IVD. Higher magnification images of boxes from (A) are indicated and shown. Partial bony endplate in cKO (D, black arrow). Round AF morphology in D (red arrow). Disrupted growth plate in E (yellow arrows). NP, nucleus pulposus; AF, annulus fibrosus; EP, endplate; GP, growth plate; VB, vertebral body

between the iAF, end plate and GP could result in the mineralized bony bridges observed in X-rays and skeletal preps, immunohistochemistry was performed for Collagen Type X comparing control and cKO tissue sections from 6-month-old mice (Figure 5A). Collagen Type X is a marker of hypertrophic differentiation and is suggestive of ectopic endochondral bone formation in these tissues. Abundant Collagen Type X staining was observed at the junction of the iAF, GP, and end plate in the area where bony bridges would be expected to form (Figure 5A, cKO image, black arrow). This indicated a change in phenotype of the cells in those regions. Collagen Type X staining was also observed in the cells of the iAF in cKO mice whereas staining was not seen in iAF from CTL mice (Figure 5A).

Morphological changes in the IVD were also accompanied by changes in proteoglycans in the ECM. Safranin-O staining revealed proteoglycan loss in the NP, iAF, and CEP, of cKO IVDs (Figure 5B). Furthermore, changes in the collagen architecture were detected in cKO IVDs via picrosirius red staining followed by polarized light microscopy (Figure 5C). Collagen architecture within and between individual lamella can be assessed using this technique. Microscopy was interpreted by analyzing birefringent intensity and the hue of birefringence in various regions of sections from the IVD of CTL and cKO mice.[32] The birefringent intensity is indicative of the degree of alignment of collagen fibers in a specimen (higher intensity is more aligned).[32] The hue of birefringence is indicative of the direction of alignment (similarly colored fibers are oriented in the same direction).[32] In healthy iAF, collagen fibers within a single lamella are oriented parallel to each other[33] (high birefringent intensity). However, the direction of collagen fibers alternates from one fiber to the next within the AF[33] (the hue of birefringence alternates between green and orange). Overall, collagen lamellae in the iAF of cKO mice were thinner than CTL mice (Figure 5D, white brackets). Alternating yellow and green hues of birefringence indicative of alternating collagen fiber directions within lamellae were not observed in cKO mice (Figure 5C, cKO image). Within the CEP of cKO mice, the basket-weave collagen architecture that was observed in CTL mice also was altered (Figure 5E, white and yellow arrows). Major alterations in the outer AF collagen architecture were not observed in cKO AF tissue (Figure 5F). This is most likely due to the fact that very little Cre recombination occurred in the oAF.

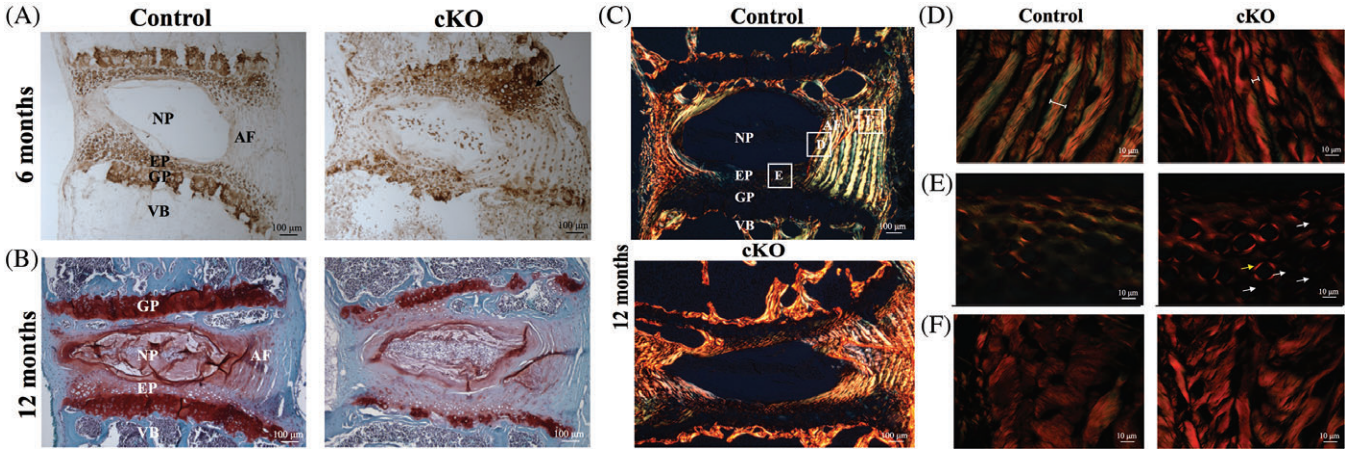


**FIGURE 5** Collagen X, proteoglycan and collagen staining. Intervertebral disc (IVD) tissue was isolated from 6- (A) or 12-month (B, C-F) old control and cKO mice. Paraffin-embedded sagittal sections were immunostained with collagen X (A) or stained with Safranin-O (B), or Picrosirius red followed by polarized light microscopy (D-F). (A). Brown staining in cKO image indicates the presence of collagen X around cells at junction of AF, GP and EP (black arrow) and within AF cells. (B) Proteoglycans are stained red. Proteoglycan loss is observed. (C) Bifringence from polarized light indicates collagen organization. Higher magnification boxes are denoted. (D) High magnification images of the inner AF from WT and cKO IVDs. Collagen bundle thinning and disorganization is observed in the inner AF of cKO mice (white bars). (E) High magnification images of the CEPs from WT and cKO IVDs. Mild collagen disorganization is observed in cKO mice (yellow and white arrows in cKO image). (F) High magnification images of the outer AF from WT and cKO mice. NP, nucleus pulposus; AF, annulus fibrosus; EP, endplate; GP, growth plate; VB, vertebral body

Overall the results suggested that Tgfbr2 is required for postnatal development and maintain of the IVD in aging mice, including development and maintenance of proteoglycan content and collagen organization.

### 3.4 | Deletion of *Tgfbr2* in Acan$^{tm(IRES\text{-}creERT2)}$-expressing cells causes phenotypic changes in the sternum

After seeing ectopic calcification in the sternum of cKO mice via skeletal preparations, further study of the sternum and ribs was performed. The SJ is a fibrocartilaginous joint located between each sternal segment (sternebrae), where CC and the sternum meet. One such joint is labeled in Figure 6A (upper left image). This joint is similar to the IVD in that it contains fibrocartilage between two bony elements (sternebrae or vertebrae). The sternebrae also have GPs on each end (Figure 6A). Functionally, it allows for gliding movements which aid in the flexibility of the rib cage. The part of the joint separating the sternebrae is maintained in mice but not in humans, where it fuses in early adulthood. Ribs and sternums from CTL and cKO mice were paraffin-embedded, sectioned coronally, and stained with H&E, Safranin-O, and picrosirius red followed by polarized light microscopy. Initially, slides were stained with H&E to investigate any changes in tissue morphology within the sternum. SJ collapse was observed in cKO mice resulting in a loss of joint space (Figure 6A, black bars in high magnification images on the right). Furthermore, the joint space was filled with tissue that histologically resembled bone (Figure 6A, black asterisks). In CTL mice, the GP contains chondrocytes organized in a columnar fashion. In contrast, in cKO mice, the GP was disorganized and discontinuous, similar to what was observed in the vertebral GPs. In some areas the GP was not present (Figure 6A). In addition to changes in tissue morphology, alterations in components of the ECM such as proteoglycans and collagen were also observed. Loss of proteoglycans as determined with Safranin O staining was observed in the remnants of the SJ of cKO mice (Figure 6B, black arrows). In addition, collagen fiber organization and orientation were greatly affected in cKO mice. Collagen fibers in WT mice within the SJ had a highly organized basket-weave appearance (Figure 6C, yellow arrow). This organization was lost in cKO mice and collagen fibers appeared to have no specific orientation (Figure 6C, white boxed regions, insets D and E in both images). The similarity in the phenotype between the fibrocartilage of the IVD and SJ suggests that TGF-β signaling in Acan-expressing cells is required for the development and maintenance of these types of fibrocartilage joints.

## 4 | DISCUSSION

In the present study, we demonstrate that conditional deletion of *Tgfbr2* postnatally in Aggrecan-expressing cells causes tissue alterations within the fibrocartilage joints of the sternum and IVD. Gene deletion in mice using CreER and tamoxifen allows for temporally regulated deletion of genes in specific tissues. Studies of this nature can address whether a gene is necessary for a particular function at a certain stage of development either embryonic or postnatal including tissue maintenance. In this study, fibrocartilage of the iAF and sternal joints did not mature or were not maintained and took on characteristics of tissue undergoing endochondral bone formation including increased expression of Type X collagen, a marker of hypertrophic differentiation. It is difficult to say if this is degeneration of the joint or defects in cell differentiation, maturation, or maintenance due to loss of TGF-β signaling. It is possible that this inappropriate endochondral bone formation resulted in the osteophytes, bony bridges and mineralization, seen in the sternum and spine on X-ray and Alizarin red-

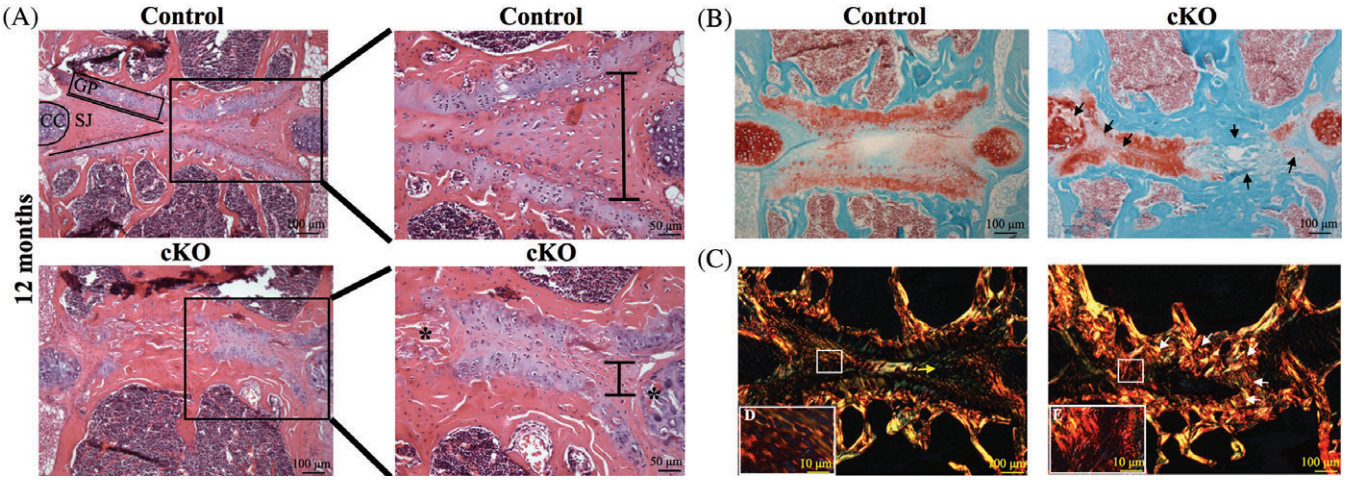


**FIGURE 6** The sternal joints are not maintained in Acan$^{tm(IRES\text{-}creERT2)}$ *Tgfbr2*$^{LoxP/LoxP}$ mice. Sternum tissue was isolated from 1-year old control and cKO mice. (A) Paraffin-embedded coronal sections were stained with hematoxylin and eosin (H&E). Low magnification images are on the left and higher magnification images of the boxed in regions are on the right. Joint space loss is observed in cKO mice when compared to control mice (black bars in 20× images). Calcification of fibrocartilaginous tissue was observed in the sternocostal joint (black asterisks in cKO 20× image). (B) Safranin-O staining. Proteoglycan loss is observed within the sternocostal joint in cKO mice (black arrows) when compared to control mice. (C) Picrosirius red staining. Collagen disorganization is observed within the SJ in cKO mice (white arrows) when compared to Contol mice. Insets (D) and (E). 100× magnification images of the boxed-in regions in both control and cKO images in panel C. Disorganization of the basket-weave appearance of the collagen fibers is observed in the cKO mice when compared to control mice. CC, costal cartilage; SJ, sternocostal joint; GP, growth plate

stained skeletal preparations. It was previously shown that Tgfbr2 is required for the embryonic development of the iAF. In the absence of Tgfbr2 the iAF was not formed and the presumptive IVD space expressed molecular markers of endochondral bone formation.[21,31] One significant observation from the present study is the alteration in cellular phenotype of AF cells into Type X collagen expressing cells between 3 and 6 months of age. It is possible that cells of the AF require TGF-β signaling to retain tissue homeostasis and prevent endochondral bone formation suggesting a role for TGF-β in cell fate decisions in both embryonic development and postnatal maturation and maintenance of the AF. TGF-β signaling could also be needed as an instructive signal to these cells to maintain a fibrous phenotype. Polymorphisms in *TGFBR2* have been associated with ossification of the posterior longitudinal ligament[18] suggesting TGF-β is required to maintain fibrous structures and prevent inappropriate mineralization in human tissue as well. In addition, the hyaline cartilage containing GP lining each of these types of joints was thin and discontinuous and prematurely replaced with bone indicating accelerated endochondral bone formation in hyaline cartilage of the spine as well.

In a previous study performed by Jin et al, *Tgfbr2* was conditionally deleted in Col2a1 expressing cells of mice at 2 weeks of age using tamoxifen.[22] They demonstrated that deletion of *Tgfbr2* in the IVD postnatally caused a disruption in columnar chondrocyte formation in the vertebral GP similar to what is observed in the Acan$^{tm(IRES\text{-}creERT2)/-}$; *Tgfbr2*$^{LoxP/LoxP}$ mice. Although Col2a-Cre was clearly active in the iAF, no obvious histological difference were observed up to 4 months of age. Acan$^{tm(IRES\text{-}creERT2)/-}$; *Tgfbr2*$^{LoxP/LoxP}$ mice were aged to 1 year and alterations in the iAF were detected by 6 months, including ectopic expression of Type X collagen. It is difficult to make conclusions about the postnatal function of *Tgfbr2* in the differently targeted cell populations (Col2a vs Acan) without aged Col2a1$^{tm1(cre/ERT2)}$ *Tgfbr2* -deleted mice.

The CEP was not efficiently targeted in the Col2a1CreER$^{T2}$; *Tgfbr2* $^{LoxP/LoxP}$ mice although the mice demonstrated thin CEP relative to controls at 3 months of age. In contrast, Acan$^{tm(IRES\text{-}creERT2)/-}$; *Tgfbr2*$^{LoxP/LoxP}$ demonstrated efficient recombination in the CEP as measured with an mTmG reporter. Thin endplates were not observed. Instead, the CEP was maintained and there was a delay in the transition to a bony endplate as the mice aged. Anatomically, in mice, a small secondary ossification center starts in the ventral-caudal aspect of the CEP.[34] The secondary ossification center spreads across the CEP to transition it to a bony endplate. In this study we observed CEP transitioning to bony endplate as early as 3 months of age with most of the endplates being bony by 12 months of age in control mice. cKO mice retained most of their CEPs even up to 12 months of age. The mechanisms of this observation are not clear and seem contradictory to TGF-β's role in inhibiting endochondral bone formation seen in other tissues presented here and elsewhere.[20,21,29,31,35] It is possible that without Tgfbr2 the organization of the secondary ossification center was disrupted so that it did not spread laterally across the CEP and instead contributed to the bony bridges observed in the X-rays and skeletal preparations.

Homeostasis of the ECM was also greatly affected by the deletion of *Tgfbr2* in Acan$^{tm(IRES\text{-}creERT2)/-}$; *Tgfbr2*$^{LoxP/LoxP}$ mice. Reduced proteoglycan staining and collagen disorganization observed in IVD could be due to alterations in matrix deposition due to attenuated TGF-β signaling. TGF-β has previously been shown to regulate the expression of proteoglycans and collagens within articular chondrocytes and IVD cells.[36–40] Conversely, it is possible that attenuation of TGF-β signaling leads to cells shifting to a catabolic state.

Although NP cells do express Col2A1, little to no Cre expression was detected in the NPs of Col2a1CreER$^{T2}$;*Tgfbr2* $^{LoxP/LoxP}$ mice described in the studies of Jin et al, and Chen et al[22,41] In contrast, Cre expression was robustly observed in the NP in Acan$^{tm(IRES\text{-}creERT2)/-}$; *Tgfbr2*$^{LoxP/LoxP}$ mice. Nevertheless, no obvious morphological changes were detected in the NPs of cKO mice compared to CTL. However, proteoglycan loss was observed in cKO NP at 12 months of age. This suggested that TGF-β signaling may only be required for certain aspects of maintenance of the aging NP that were not explored here.

TGF-β signaling may not be the only pathway necessary to maintain IVD tissue. Various members of the TGF-β superfamily such as GDF[42] and BMP[43] have been shown to be involved in the development of the IVD. Future studies could investigate their potential role in postnatal growth and maintenance of the IVD tissue. It is clear, however, that TGF-β signaling is an important factor in the postnatal development and maintenance of the IVD. Elucidating the mechanism for how TGF-β signaling regulates maintenance of the IVD could be helpful in the prevention of disc degeneration or conditions of inappropriate mineralization and vertebral fusion.

## ACKNOWLEDGEMENTS

The authors would like to thank Phil Sohn and Swetha Surianarayanan for their help in tissue section and staining. An additional thank you to the UAB Small Animal Phenotyping Core supported by the NIH Diabetes Research Center P30DK079626 for their assistance in the X-ray analysis of the mice. This work was supported by an NIH R01 AR053860 to RS and the DART training grant NIH NIDCR T-90DE022736 to BA.

## Author contributions

B.A. and R.S. conceived and designed the study. B.A. and C.L. acquired, analyzed, and interpreted the data. B.A. and R.S. wrote the article. RS revised the article for intellectual content. All authors approved the final version of the article. All authors take responsibility for the integrity of the work.

## Conflict of Interest

The authors do not have any conflict of interests to declare.

## ORCID

*Rosa Serra* http://orcid.org/0000-0002-4832-7366

## REFERENCES

1. Chang H, Brown CW, Matzuk MM. Genetic analysis of the mammalian transforming growth factor-beta superfamily. *Endocr Rev*. 2002;*23*(6):787-823.
2. Massague J, Blain SW, Lo RS. TGFbeta signaling in growth control, cancer, and heritable disorders. *Cell*. 2000;*103*(2):295-309.
3. Newfeld SJ, Wisotzkey RG, Kumar S. Molecular evolution of a developmental pathway: phylogenetic analyses of transforming growth factor-beta family ligands, receptors and Smad signal transducers. *Genetics*. 1999;*152*(2):783-795.
4. Laiho M, Weis MB, Massague J. Concomitant loss of transforming growth factor (TGF)-beta receptor types I and II in TGF-beta-resistant cell mutants implicates both receptor types in signal transduction. *J Biol Chem*. 1990;*265*(30):18518-18524.
5. Ruberte E, Marty T, Nellen D, Affolter M, Basler K. An absolute requirement for both the type II and type I receptors, punt and thick veins, for dpp signaling in vivo. *Cell*. 1995;*80*(6):889-897.
6. Wrana JL, Attisano L, Carcamo J, et al. TGF beta signals through a heteromeric protein kinase receptor complex. *Cell*. 1992;*71*(6):1003-1014.
7. Wrana JL, Attisano L, Wieser R, Ventura F, Massague J. Mechanism of activation of the TGF-beta receptor. *Nature*. 1994;*370*(6488):341-347.
8. Humzah MD, Soames RW. Human intervertebral disc: structure and function. *Anat Rec*. 1988;*220*(4):337-356.
9. Lundon K, Bolton K. Structure and function of the lumbar intervertebral disk in health, aging, and pathologic conditions. *J Orthop Sports Phys Ther*. 2001;*31*(6):291-303; discussion 304-296.
10. Raj PP. Intervertebral disc: anatomy-physiology-pathophysiology-treatment. *Pain Pract*. 2008;*8*(1):18-44.
11. Cox M, Serra R. Development of the intervertebral disc. In: Shapiro IM, Risbud MV, eds. *The Intervertebral Disc: Molecular and Structural Studies of the Disc in Health and Disease*. Springer, New York City, NY; 2014.
12. Yamada Y, Okuizumi H, Miyauchi A, Takagi Y, Ikeda K, Harada A. Association of transforming growth factor beta1 genotype with spinal osteophytosis in Japanese women. *Arthritis Rheum*. 2000;*43*(2):452-460.
13. Seki S, Kawaguchi Y, Chiba K, et al. A functional SNP in CILP, encoding cartilage intermediate layer protein, is associated with susceptibility to lumbar disc disease. *Nat Genet*. 2005;*37*(6):607-612.
14. Loeys BL, Chen J, Neptune ER, et al. A syndrome of altered cardiovascular, craniofacial, neurocognitive and skeletal development caused by mutations in TGFBR1 or TGFBR2. *Nat Genet*. 2005;*37*(3):275-281.
15. Matyas G, Naef P, Tollens M, Oexle K. De novo mutation of the latency-associated peptide domain of TGFB3 in a patient with overgrowth and Loeys-Dietz syndrome features. *Am J Med Genet A*. 2014;*164A*(8):2141-2143.
16. Valenzuela I, Fernandez-Alvarez P, Munell F, et al. Arthrogryposis as neonatal presentation of Loeys-Dietz syndrome due to a novel TGFBR2 mutation. *Eur J Med Genet*. 2017;*60*(6):303-307.
17. Horikoshi T, Maeda K, Kawaguchi Y, et al. A large-scale genetic association study of ossification of the posterior longitudinal ligament of the spine. *Hum Genet*. 2006;*119*(6):611-616.
18. Jekarl DW, Paek CM, An YJ, et al. TGFBR2 gene polymorphism is associated with ossification of the posterior longitudinal ligament. *J Clin Neurosci*. 2013;*20*(3):453-456.
19. MacFarlane EG, Haupt J, Dietz HC, Shore EM. TGF-beta family signaling in connective tissue and skeletal diseases. *Cold Spring Harb Perspect Biol*. 2017;*9*(11):667-724.
20. Serra R, Johnson M, Filvaroff EH, et al. Expression of a truncated, kinase-defective TGF-beta type II receptor in mouse skeletal tissue promotes terminal chondrocyte differentiation and osteoarthritis. *J Cell Biol*. 1997;*139*(2):541-552.
21. Baffi MO, Slattery E, Sohn P, Moses HL, Chytil A, Serra R. Conditional deletion of the TGF-beta type II receptor in Col2a expressing cells results in defects in the axial skeleton without alterations in chondrocyte differentiation or embryonic development of long bones. *Dev Biol*. 2004;*276*(1):124-142.
22. Jin H, Shen J, Wang B, Wang M, Shu B, Chen D. TGF-beta signaling plays an essential role in the growth and maintenance of intervertebral disc tissue. *FEBS Lett*. 2011;*585*(8):1209-1215.
23. Henry SP, Jang CW, Deng JM, Zhang Z, Behringer RR, de Crombrugghe B. Generation of aggrecan-CreERT2 knockin mice for inducible Cre activity in adult cartilage. *Genesis*. 2009;*47*(12):805-814.
24. Chytil A, Magnuson MA, Wright CV, Moses HL. Conditional inactivation of the TGF-beta type II receptor using Cre:Lox. *Genesis*. 2002;*32*(2):73-75.
25. Muzumdar MD, Tasic B, Miyamichi K, Li L, Luo L. A global double-fluorescent Cre reporter mouse. *Genesis*. 2007;*45*(9):593-605.
26. Selby PB. A rapid method for preparing high quality alizarin stained skeletons of adult mice. *Stain Technol*. 1987;*62*(3):143-146.

27. Bushell GR, Ghosh P, Taylor TF, Akeson WH. Proteoglycan chemistry of the intervertebral disks. *Clin Orthop Relat Res*. 1977;*129*: 115-123.
28. Jahnke MR, McDevitt CA. Proteoglycans of the human intervertebral disc. Electrophoretic heterogeneity of the aggregating proteoglycans of the nucleus pulposus. *Biochem J*. 1988;*251*(2):347-356.
29. Seo HS, Serra R. Deletion of Tgfbr2 in Prx1-cre expressing mesenchyme results in defects in development of the long bones and joints. *Dev Biol*. 2007;*310*(2):304-316.
30. Baffi MO, Moran MA, Serra R. Tgfbr2 regulates the maintenance of boundaries in the axial skeleton. *Dev Biol*. 2006;*296*(2):363-374.
31. Sohn P, Cox M, Chen D, Serra R. Molecular profiling of the developing mouse axial skeleton: a role for Tgfbr2 in the development of the intervertebral disc. *BMC Dev Biol*. 2010;*10*:29.
32. Nerurkar NL, Baker BM, Sen S, Wible EE, Elliott DM, Mauck RL. Nanofibrous biologic laminates replicate the form and function of the annulus fibrosus. *Nat Mater*. 2009;*8*(12):986-992.
33. Cassidy JJ, Hiltner A, Baer E. Hierarchical structure of the intervertebral disc. *Connect Tissue Res*. 1989;*23*(1):75-88.
34. Zhang Y, Lenart BA, Lee JK, et al. Histological features of endplates of the mammalian spine: from mice to men. *Spine (Phila Pa 1976)*. 2014; *39*(5):E312-E317.
35. Serra R, Karaplis A, Sohn P. Parathyroid hormone-related peptide (PTHrP)-dependent and -independent effects of transforming growth factor beta (TGF-beta) on endochondral bone formation. *J Cell Biol*. 1999;*145*(4):783-794.
36. Gruber HE, Fisher EC Jr., Desai B, Stasky AA, Hoelscher G, Hanley EN Jr. Human intervertebral disc cells from the annulus: three-dimensional culture in agarose or alginate and responsiveness to TGF-beta1. *Exp Cell Res*. 1997;*235*(1):13-21.
37. Lee YJ, Kong MH, Song KY, Lee KH, Heo SH. The relation between Sox9, TGF-beta1, and proteoglycan in human intervertebral disc cells. *J Korean Neurosurg Soc*. 2008;*43*(3):149-154.
38. Redini F, Galera P, Mauviel A, Loyau G, Pujol JP. Transforming growth factor beta stimulates collagen and glycosaminoglycan biosynthesis in cultured rabbit articular chondrocytes. *FEBS Lett*. 1988;*234*(1): 172-176.
39. Galera P, Vivien D, Pronost S, et al. Transforming growth factor-beta 1 (TGF-beta 1) up-regulation of collagen type II in primary cultures of rabbit articular chondrocytes (RAC) involves increased mRNA levels without affecting mRNA stability and procollagen processing. *J Cell Physiol*. 1992;*153*(3):596-606.
40. Morales TI, Roberts AB. Transforming growth factor beta regulates the metabolism of proteoglycans in bovine cartilage organ cultures. *J Biol Chem*. 1988;*263*(26):12828-12831.
41. Chen M, Lichtler AC, Sheu TJ, et al. Generation of a transgenic mouse model with chondrocyte-specific and tamoxifen-inducible expression of Cre recombinase. *Genesis*. 2007;*45*(1):44-50.
42. Li X, Leo BM, Beck G, Balian G, Anderson GD. Collagen and proteoglycan abnormalities in the GDF-5-deficient mice and molecular changes when treating disk cells with recombinant growth factor. *Spine (Phila Pa 1976)*. 2004;*29*(20):2229-2234.
43. Zieba J, Forlenza KN, Khatra JS, et al. TGFbeta and BMP dependent cell fate changes due to loss of Filamin B produces disc degeneration and progressive vertebral fusions. *PLoS Genet*. 2016;*12*(3):e1005936.


**How to cite this article:** Alkhatib B, Liu C, Serra R. Tgfbr2 is required in Acan-expressing cells for maintenance of the intervertebral and sternocostal joints. *JOR Spine*. 2018;1:e1025. https://doi.org/10.1002/jsp2.1025